COLREGS-Compliant collision avoidance for physically coupled multi-vessel systems with distributed MPC

Du, Z.; Negenborn, Rudy R.; Reppa, Vasso

DOI
10.1016/j.oceaneng.2022.111917

Publication date
2022

Document Version
Final published version

Published in
Ocean Engineering

Ocean Engineering 260 (2022) 111917

Contents lists available at ScienceDirect

Ocean Engineering

journal homepage: www.elsevier.com/locate/oceaneng

COLREGS-Compliant collision avoidance for physically coupled multi-vessel systems with distributed MPC

Zhe Du *, Rudy R. Negenborn, Vasso Reppa

Department of Maritime and Transport Technology, Delft University of Technology, Mekelweg 2, 2628 CD, Delft, The Netherlands

ARTICLE INFO

Keywords:
Cooperative control
Distributed MPC
Collision avoidance
Multi-vessel systems
Ship towing

ABSTRACT

This paper proposes a distributed control scheme for autonomous tugboats to tow a ship in a restricted water traffic environment ensuring collision avoidance while being compliant with maritime regulation called COLREGS. The complex problem is cooperatively solved by addressing three sub-optimization problems. The first is to optimize the towing forces and angles for solving ship waypoint following and collision avoidance problems. The second is to optimize the tug thruster forces and moment for solving the tug online trajectory tracking and collision avoidance problems. The third is to optimize the Lagrange Multipliers for solving the consensus problem between the ship and tugs. The distributed control architecture follows the Model Predictive Control (MPC) strategy using the Altering Direction Method of Multipliers (ADMM). Simulation experiments indicate that the proposed control scheme can deal with static and dynamic obstacles in restricted waterways for a physically interconnected multi-vessel system executing the towing process, and the collision avoidance complies with COLREGS rules.

1. Introduction

As an essential requirement for autonomy, collision avoidance plays an important role in autonomous vehicle systems, like Unmanned Aerial Vehicles (UAVs), Unmanned Ground Vehicles (UGVs), and Autonomous Surface Vessels (ASVs), to ensure the safety of carrying out missions (Zhang et al., 2021). In the water traffic environment, all the vessels that take actions of avoidance should comply with standards of global regulations called "The International Regulations for Preventing Collisions at Sea", shortly COLREGS (Cockcroft and Lameijer, 2003).

Although COLREGS have been designed to be followed by humans, they must be obeyed during the operations of autonomous vessels in order to guarantee their lawfulness at sea (Campbell et al., 2012). Research works usually combine rules 13–17 (the specific actions that the give-way vessel should take) with classical guidance or control methods to make the ASV avoid obstacles. In Johansen et al. (2016), Trym et al. (2020), Hagen et al. (2018), scholars propose a COLREG-compliant model predictive control method for ship collision avoidance. Research works (Zaccone, 2021) and Chiang and Tapia (2018) focus on path planning of ASVs and propose COLREG-compliant RRT optimal planning strategy. In Ahmed et al. (2021), a Fuzzy-logic based conflict detection and resolution algorithm is proposed for situations of multiple ships, where the fuzzy rules are defined in accordance with the COLREGs. Other research works use the methods of Velocity Obstacle (VO) (Huang et al., 2019) and Artificial Potential Fields (APF) (Lyu and Yin, 2018) combined with COLREG rules to address collision avoidance problems for ASVs.

In recent years, the increasing complexity and scale of missions have motivated the deployment of multi-vehicle systems. Correspondingly, collision avoidance of the multi-vehicle system becomes more challenging. There are two types of such a system according to the way of connection: Cyber-connected and Physical-connected. For a cyber-connected system all vehicles are clustered in a certain range maintaining a safe distance, and the connection is realized through a digital network. The physical-connected system often contains a physical link (like a cable or direct attachment) between vehicles. Compared to the cyber-connected system, this type has less ability of maneuvering and more constraints on dynamics.

Table 1 presents the classification of avoidance strategies for multi-vehicle systems considering the type of vehicles and connection, as well as control architecture and obstacle attributes.

For multi-ASV systems, collision avoidance research focuses on the type of cyber-connected. Researchers usually arrange a specific formation to coordinate multiple ASVs. The typical one is the triangle formation composed of three vessels (Kim et al., 2016; Hinostroza et al., 2019). The triangle formation can easily adopt the leader–follower cooperative control strategy that maintains the vessel formation in premises of avoiding collision with islands and coast. For more than

* Corresponding author.
E-mail address: duzhe9224@foxmail.com (Z. Du).

https://doi.org/10.1016/j.oceaneng.2022.111917
Received 17 July 2021; Received in revised form 26 March 2022; Accepted 3 July 2022
Available online 16 July 2022

Table 1
Classification of control & avoidance methods for multi-vehicle system.

Research article	Type of vehicles			Type of connection		Control architecture		Obstacle attributes		Strategies[a]
	ASV	UGV	UAV	Cyber	Physical	Centralized	Distributed	Static	Dynamic	
Kim et al. (2016)	✓			✓			✓	✓		LOS + HS
Hinostroza et al. (2019)	✓			✓			✓	✓	✓	VF + FC + COLREGS
Arrichiello et al. (2006)	✓			✓			✓	✓		NSBC
Qin et al. (2017)	✓			✓			✓	✓		TC + APF
Chen et al. (2018)	✓			✓			✓	✓		DMPC
Li et al. (2019)		✓			✓	✓		✓		OC + GT
Zips et al. (2015)		✓			✓	✓		✓		OC + HS
Yuan (2017)		✓			✓	✓		✓		PSO + GT
Raghuwaiya et al. (2014)		✓			✓	✓		✓		APF + OSR
Eoh et al. (2016)		✓			✓		✓	✓		APF + EDF
Fink et al. (2008)		✓			✓		✓	✓		BC + VF
Rossomando et al. (2020), Rosales et al. (2019)			✓		✓	✓		✓		NN + NSBC
Lee (2015)			✓		✓	✓		✓		GT + VG
Gimenez et al. (2018)			✓		✓	✓		✓		APF + NSBC
Tartaglione et al. (2017)			✓		✓		✓	✓		MPC
Lee et al. (2018)			✓		✓		✓	✓		RRT + DMPs + AFP
Du et al. (2021b)	✓				✓	✓		✓	✓	MPC + COLREGS
This paper	✓				✓		✓	✓	✓	**DMPC + COLREGS**

[a]APF: Artificial Potential Field; (NS)BC: (Null-Space based) Behavioral Control; DMPs: Dynamic Movement Primitives; EDF: Electric Dipole Field; FC: Fuzzy Control; FMS: Fast Marching Square; GT: Graph Theory; HS: Heuristic-based Searching; LOS: Line-Of-Sight; (D)MPC: (Distributed) Model Predictive Control; NN: Neural Networks; OC: Optimal Control; OSR: Obstacle Space Representation; PSO: Particle Swarm Optimization; RRT: Rapidly exploring Random Tree; TC: Task-based Control; VG: Voronoi Graph; VF: Vector Field.

three vessels, the reconfigurable formation can be applied (Arrichiello et al., 2006; Qin et al., 2017). This type of formation is often combined with a task-based (or behavior-based) cooperative control strategy in which a collision-avoidance task is carried out by changing the formation. Alternatively, a line formation (or a vessel-train formation) is proposed to deal with the collisions in a narrow waterway of port areas (Chen et al., 2018).

Since the physical-connected multi-vehicle systems have less maneuverability that makes their control challenging, research works in collision avoidance of physical-connected systems are mainly related to the relatively well-developed autonomous vehicles: Multiple ground and aerial vehicle systems. For ground vehicles, some research works have focused on tractor–trailer systems which consist of a driven tractor and several passive trailers (Li et al., 2019; Zips et al., 2015; Yuan, 2017; Raghuwaiya et al., 2014). In these works, the collision avoidance strategy is commonly based on combining optimization methods with graph theory. Several researchers have been working on collision avoidance of swarms of wheeled robots (Eoh et al., 2016; Fink et al., 2008). The collision avoidance of an object-caging system (Eoh et al., 2016) and an object-pushing system (Fink et al., 2008) has been realized by using the potential (vector) field theory. For aerial vehicles, the multi-UAV system is usually applied for payload transportation (Rossomando et al., 2020; Lee, 2015; Gimenez et al., 2018; Rosales et al., 2019; Tartaglione et al., 2017; Lee et al., 2018). In this case, two or three UAVs are used to transport a payload connected by cables. By taking the avoidance as a part of the control objectives or constraints, the payload transportation mission and collision avoidance can be both achieved. Some scholars take the distance between the collision and each UAV and payload as constraints to keep the obstacles out of a certain range (Rossomando et al., 2020; Gimenez et al., 2018; Rosales et al., 2019; Tartaglione et al., 2017), while others first utilize a searching algorithm to plan a collision-free path for the multi-UAV system, then this path is considered as a reference to follow (Lee, 2015; Lee et al., 2018).

From the point of the control architecture, the majority of the research works of multi-ASV systems uses a distributed structure. Although the distributed architecture has been mostly applied to cyber connected ASVs, in the case of the multi-UGV and multi-UAV systems, the centralized control architecture is more applied for such strong interconnected (physical-connected) systems. However, some research works adopt the distributed control architecture into their physical-connected multi-UGV (Eoh et al., 2016) or multi-UAV (Tartaglione et al., 2017; Lee et al., 2018) system to achieve collision avoidance. The advantages of the easier implementation, lower computation time, scalable application scenarios, and tolerance to failures make the distributed control superior over other architectures (Negenborn and Maestre, 2013; Du et al., 2021a).

Regarding the types of obstacles the multi-vehicle system dealing with, most research works only consider static obstacles in their environment. Few research (Hinostroza et al., 2019; Du et al., 2021b) concerns both static and dynamic obstacles and considers COLREGS rules in the avoidance process. To the authors' best knowledge, there has been no research on collision avoidance of the physical-connected multi-ASV systems.

The goal and the main contribution of this work is the design of a distributed control scheme capable of avoiding collisions for a physically interconnected multi-ASV system performing a towing process. Collision avoidance problems consist of three parts: Motion prediction, conflict detection, and conflict resolution (Huang et al., 2020). This paper focuses on the last two parts, and the motion prediction is out of our research scope. As shown in the last two rows of Table 1, in previous research we have investigated a centralized cooperative control scheme for a ship-towing system to deal with collision avoidance (Du et al., 2021b). In this paper, the proposed control scheme is based on a distributed control architecture, dealing with both static and dynamic obstacles in restricted waterways, and the avoidance operation adheres to COLREGS (rules 13–17).

The remainder of this paper is organized as follows. Section 2 formulates the main problem of our research and models of the towing system. The design of the proposed control scheme is given in Section 3 by first introducing the COLREGS-compliant guidance system, then formulating the centralized control problem, and finally designing the ADMM-based distributed MPC scheme. In Section 4, simulation experiments are carried out for representative situations to illustrate the potential of the proposed scheme. Conclusions and future research directions are given in Section 5.

2. Problem statement and system modeling

The goal of this work is to design a distributed control scheme for a physical-connected multi-vessel autonomous towing system in a congested water traffic environment. The towing system consists of three vessels: Two ASVs are the tugboats located at the front and back to provide power; a ship located in the middle position connected with the two ASVs by a towing line is the manipulated object. The proposed control scheme requires the coordination of the two ASVs to cooperatively manipulate the ship to the desired position with the desired heading without collisions while complying with COLREGS.

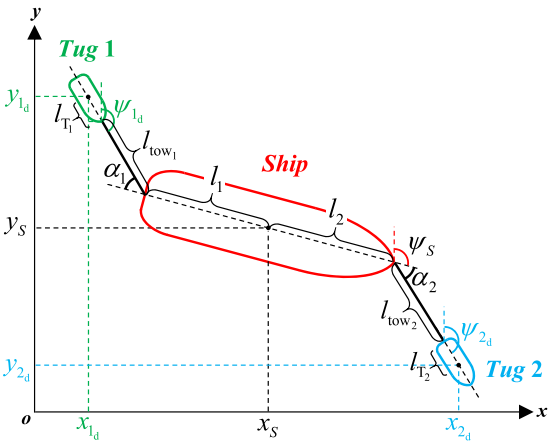

Fig. 1. Configuration of the towing system.

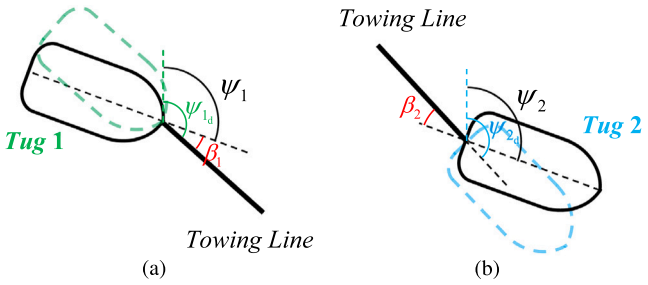

Fig. 2. Relationship among tug angle β_i, desired tug heading ψ_{i_d} and actual tug heading ψ_i: (a) Tug 1; (b) Tug 2.

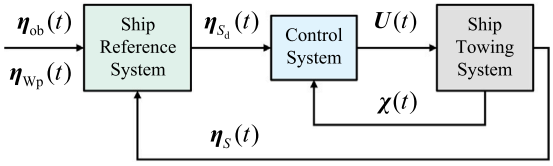

Fig. 3. Main systems for performing the towing process.

2.1. Mathematical model of the vessel

The 3-DoF (degree of freedom) maneuvering model (Fossen, 2011) considering the kinematics and kinetics of the vessels in the towing system is expressed as:

$$\begin{aligned}&\dot{\boldsymbol{\eta}}_*(t) = \boldsymbol{R}\left(\psi_*(t)\right)\boldsymbol{\nu}_*(t)\\&\boldsymbol{M}_*\dot{\boldsymbol{\nu}}_*(t) + \boldsymbol{C}_*\left(\boldsymbol{\nu}_*(t)\right)\boldsymbol{\nu}_*(t) + \boldsymbol{D}_*\boldsymbol{\nu}_*(t) = \boldsymbol{\tau}_*(t),\end{aligned} \tag{1}$$

where $*$ stands for S (ship) or i ($i = 1, 2$) (tug); $\boldsymbol{\eta}(t) = [x(t)\ \ y(t)\ \ \psi(t)]^{\mathrm{T}} \in \mathbb{R}^3$ is the position vector in the world frame (North-East-Down) including ship position coordinates ($x(t)$, $y(t)$) and heading $\psi(t)$; $\boldsymbol{\nu}(t) = [u(t)\ \ v(t)\ \ r(t)]^{\mathrm{T}} \in \mathbb{R}^3$ is the velocity vector in the Body-fixed frame containing the velocity of surge $u(t)$, sway $v(t)$ and yaw $r(t)$; $\boldsymbol{R} \in \mathbb{R}^{3\times3}$ is the rotation matrix from the body frame to the world frame, which is a function of heading; $\boldsymbol{M} \in \mathbb{R}^{3\times3}$, $\boldsymbol{C} \in \mathbb{R}^{3\times3}$ and $\boldsymbol{D} \in \mathbb{R}^{3\times3}$ are the mass (inertia), Coriolis-Centripetal and damping matrix, respectively; $\boldsymbol{\tau}(t) = [\tau_{\mathrm{u}}(t)\ \ \tau_{\mathrm{v}}(t)\ \ \tau_{\mathrm{r}}(t)]^{\mathrm{T}} \in \mathbb{R}^3$ is the controllable input referring to the forces $\tau_{\mathrm{u}}(t)$, $\tau_{\mathrm{v}}(t)$ and moment $\tau_{\mathrm{r}}(t)$ offered by actuators in the Body-fixed frame.

The controllable inputs of the ship (the manipulated vessel in the middle) denoted by $\boldsymbol{\tau}_S$ are the forces from the towing lines applied by the two tugs (see Du et al. (2020) for details on modeling of the ship towing system), which can be expressed as:

$$\begin{aligned}&\boldsymbol{\tau}_S(t) = \boldsymbol{\tau}_{S_1}(t) + \boldsymbol{\tau}_{S_2}(t) = \sum_{i=1}^{2}\boldsymbol{B}_S\left(\alpha_i(t)\right)F_i(t)\\&\boldsymbol{B}_S = \begin{bmatrix}\cos\left(\alpha_i(t)\right)\\ \sin\left(\alpha_i(t)\right)\\ l_i\sin\left(\alpha_i(t)\right)\end{bmatrix}\qquad (i = 1, 2),\end{aligned} \tag{2}$$

where $F_i(t)$ represents the towing forces; $\boldsymbol{B} \in \mathbb{R}^3$ is the configuration matrix which is a function of the towing angle ($\alpha_i(t)$), l_i is the distance from the center of gravity of the ship to the ship stern (l_1) or the ship bow (l_2). The term $\alpha_i(t)$ and l_i are depicted in Fig. 1.

The controllable inputs of the ith tug (the ASV located at the front and back) denoted by $\boldsymbol{\tau}_i$ consist of the reaction towing force and the thruster forces (omnidirectional forces generated by azimuth thrusters (Hensen, 2003)) expressed as:

$$\begin{aligned}&\boldsymbol{\tau}_i(t) = \boldsymbol{B}_i\left(\beta_i(t)\right)F_i'(t) + \boldsymbol{\tau}_{T_i}(t)\\&\boldsymbol{B}_i = \begin{bmatrix}\cos\left(\beta_i(t)\right)\\ \sin\left(\beta_i(t)\right)\\ l_{T_i}\sin\left(\beta_i(t)\right)\end{bmatrix}\qquad (i = 1, 2),\end{aligned} \tag{3}$$

where $\boldsymbol{B}_i \in \mathbb{R}^3$ is the configuration matrix of the tug i; $\boldsymbol{\tau}_{T_i}(t) \in \mathbb{R}^3$ is the forces and moment to move the tug i; $\beta_i(t)$ is the tug angle; l_{T_i} is the distance from the center of gravity of the tug to the tug stern (l_{T_2}) or the tug bow (l_{T_1}) (see Fig. 1); $F_i'(t)$ is the force applied through a controlled winch onboard the tugboat to the towline, assuming no force loss on the towline, then $F_i'(t) \equiv F_i(t)$. In this work, we do not consider the low-level winch control and the detailed model of the force F_i as a function of the elastic elongation and the generalized stiffness that depends on the material, diameter and the strand construction of the towline.

2.2. Configuration of the towing system

Assuming that there is a desired elongation of the towline l_{tow_i} that guarantees the action of the restoring force and the collision avoidance between the two vessels, the configuration for the towing system according to the geometrical relationship between the ship and tugs can be defined as shown in Fig. 1 (Du et al., 2020). Thus, for $i = 1, 2$, the desired position and heading of tug i ($\boldsymbol{\eta}_{i_{\mathrm{d}}}(t) = [x_{i_{\mathrm{d}}}(t)\ \ y_{i_{\mathrm{d}}}(t)\ \ \psi_{i_{\mathrm{d}}}(t)]^{\mathrm{T}}$) is determined by

$$\begin{aligned}\boldsymbol{\eta}_{i_{\mathrm{d}}}(t) = {}&\boldsymbol{\eta}_S(t) + (l_{\mathrm{tow}_i} + l_{\mathrm{T}_i})\boldsymbol{E}_i\left(\psi_S(t), \alpha_i(t)\right) +\\&l_i\boldsymbol{F}_i\left(\psi_S(t)\right) + \alpha_i(t)[0\ \ 0\ \ 1]^{\mathrm{T}},\end{aligned} \tag{4}$$

where $\boldsymbol{\eta}_S(t) = [x_S(t)\ \ y_S(t)\ \ \psi_S(t)]^{\mathrm{T}} \in \mathbb{R}^3$ is the position and heading of the ship; $\boldsymbol{E}_i \in \mathbb{R}^3$ and $\boldsymbol{F}_i \in \mathbb{R}^3$ are the vectors related to the heading of the ship and the towing angles, formulated as:

$$\boldsymbol{E}_i = (-1)^i\begin{bmatrix}\sin\left(\psi_S(t) + \alpha_i(t)\right)\\ \cos\left(\psi_S(t) + \alpha_i(t)\right)\\ 0\end{bmatrix}, \tag{5}$$

$$\boldsymbol{F}_i = (-1)^i\begin{bmatrix}\sin\left(\psi_S(t)\right)\\ \cos\left(\psi_S(t)\right)\\ 0\end{bmatrix}. \tag{6}$$

It is noted that there might be some deviation between the actual and desired heading of the tugs, which is caused by the tug angle $\beta_i(t)$ (shown in Fig. 2). Thus, the tug angle of the tug i can be calculated by:

$$\beta_i(t) = \alpha_i(t) + \psi_S(t) - \psi_i(t). \tag{7}$$

3. Distributed cooperative control scheme

As shown in Fig. 3, there are three main systems in performing the towing process. According to the information of obstacles ($\boldsymbol{\eta}_{\mathrm{ob}}(t)$), the predefined waypoints ($\boldsymbol{\eta}_{\mathrm{Wp}}(t)$), and the current position of the ship ($\boldsymbol{\eta}_S(t)$), the ship reference system provides the desired ship position

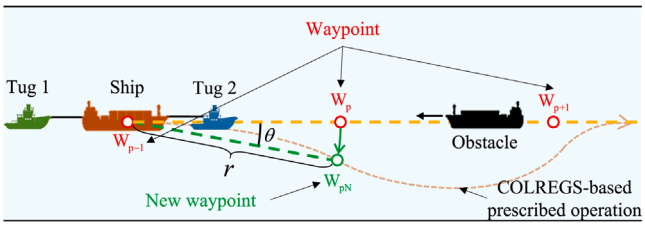

Fig. 4. An example of prescribed actions for the head-on situation that a towing system should take.

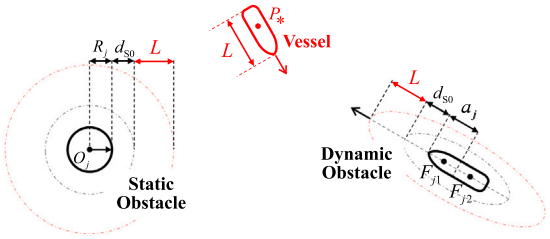

Fig. 5. Distance of different obstacles.

and heading ($\boldsymbol{\eta}_{Sd}(t)$) to the control system. The control system uses the above data and current states of the ship and two tugs ($\chi(t)$) to calculate the control orders ($\boldsymbol{U}(t)$) that coordinates the two tugs to manipulate the ship and avoid obstacles.

3.1. Ship reference system

The ship reference system is designed to make the towing system adhere to the COLREGS applicable to a physically-connected multi-vessel system. The COLREGS, which is made for a single vessel, include 41 rules divided into six parts, where rules 13–17 in Part B (Steering and Sailing Rules) explicitly prescribe actions that a vessel should take when encountering collision risk. Rules 13 to 15 provide definitions and operations of the three situations that a single vessel may encounter: Overtaking, head-on, and crossing. Rule 16 describes the generic actions that the give-way vessels should take, and Rule 17 indicates the actions that the stand-on vessels should take.

Considering the characteristics of the physically-connected multi-vessel system with restricted maneuverability and relatively low speed, to make sure the towing system safe we assume that the operations taken by the autonomous tugboat will not make the own ship overtaking other target vessels (as a result, by default, Rule 13 is satisfied). So the collision avoidance focuses on the head-on (Rule 14) and crossing (Rule 15) situations. Meanwhile, we define a detection distance to the obstacle (explained next) to adjust the role of the towing system: when the obstacle further away than such a distance, the towing system will have the role of "stand-on vessel" (Rule 17); otherwise, the risk is considered to be unrelieved and the towing system as having the role of a "give-way vessel", which has to take avoidance action (Rule 16).

The prescribed actions in Rules 14 and 15 indicate that the give-way vessel should steer to the starboard side (right) so that each vessel passes on the port side (left) of each other. However, for the ship in the towing system, its movements are controlled by the two connected tugs. So the prescribed operations should be formulated in a different way.

In maritime practice, a set of fixed waypoints are usually applied in the towing process to guide it to its goal. If there are no dynamic obstacles, the system should follow this predefined path to get to the destination; otherwise, the potential collisions will happen on this path. In the presence of dynamic obstacles, these waypoints can be used as an alternative way for the COLREGS-based prescribed operations. As shown in Fig. 4, when encountering obstacles, the red dotted curve should be the prescribed operation according to COLREGS. This operation of starboard steering can be equivalently converted to a clockwise waypoint altering (the current goal waypoint W_p is altered by a new waypoint W_{pN}). The criteria for such a deviation from the nominal path is determined by comparing the detection distance d_D and obstacle distance $d_{ob}(t)$, expressed as:

$$\begin{cases} \boldsymbol{\eta}_{Sd}(t) = \boldsymbol{\eta}_{Sp}, & \text{if } \ d_{ob}(t) > d_D \\ \boldsymbol{\eta}_{Sd}(t) = \boldsymbol{\eta}_{Sn}, & \text{if } \ d_{ob}(t) \le d_D \\ d_{ob}(t) = \min\left\{ d_{Sj}(t), d_{1j}(t), d_{2j}(t) \right\}, \end{cases} \tag{8}$$

where $\boldsymbol{\eta}_{Sp}$ and $\boldsymbol{\eta}_{Sn}$ are the predefined and the new (updated) position references of waypoint p, respectively. The parameter detection distance d_D is determined by the range sensors. The terms $d_{Sj}(t)$, $d_{1j}(t)$, and $d_{2j}(t)$ are the actual distance from the obstacle j to the manipulated ship, to the tug 1, and to the tug 2, respectively. Their values are calculated according to the attributes of the obstacle: the static obstacle is treated as a circle, and the dynamic obstacle is treated as an ellipse. As seen in Fig. 5, for $*$ represents the own vessel, the obstacle distance is then expressed as:

$$\begin{aligned} d_{*j}(k) &= \begin{cases} \overline{P_*O_j} & \text{for } j \text{ is circle obstacle} \\ \overline{P_*F_{j1}} + \overline{P_*F_{j2}} & \text{for } j \text{ is ellipse obstacle} \end{cases} \\ \overline{P_*O_j} &= \sqrt{(x_* - x_{Oj})^2 + (y_* - y_{Oj})^2} \\ \overline{P_*F_{j1}} &= \sqrt{(x_* - x_{Fj1})^2 + (y_* - y_{Fj1})^2} \\ \overline{P_*F_{j2}} &= \sqrt{(x_* - x_{Fj2})^2 + (y_* - y_{Fj2})^2} \end{aligned} \tag{9}$$

where (x_*, y_*) is the coordinates of the own vessel, (x_{Oj}, y_{Oj}) is the coordinates of the static obstacle, (x_{Fj1}, y_{Fj1}) and (x_{Fj2}, y_{Fj2}) are the coordinates of the two focuses for dynamic obstacle. Condition (8) implies that the risk of collision is defined considering all three vessels as an interconnected system and the collision avoidance should be guaranteed by all vessels.

The new waypoint is determined by an arc of the circle with center the last predefined waypoint $(p-1)$ and radius the distance between $p-1$ and p. The direction is clockwise for the operations of starboard steering. The planar coordinates (x_{Sn}, y_{Sn}) of the new waypoint can be computed as:

$$\begin{aligned} \begin{bmatrix} x_{Sn} \\ y_{Sn} \end{bmatrix} &= \begin{bmatrix} x_{Sp-1} \\ y_{Sp-1} \end{bmatrix} + r \cdot \begin{bmatrix} \sin(\theta) \\ \cos(\theta) \end{bmatrix} \\ r &= \left\| \begin{bmatrix} x_{Sp-1} \\ y_{Sp-1} \end{bmatrix} - \begin{bmatrix} x_{Sp} \\ y_{Sp} \end{bmatrix} \right\|_2, \end{aligned} \tag{10}$$

where (x_{Sp-1}, y_{Sp-1}) is the coordinates of the last predefined waypoint; (x_{Sp}, y_{Sp}) is the coordinates of the current predefined waypoint; r is the distance between the above two waypoints; θ is the altering angle ($\theta > 0°$ for clockwise rotation). The reference heading angle of the new waypoint can be expressed as

$$\psi_{Sn} = \psi_{Sp} + \theta, \tag{11}$$

where ψ_{Sp} is the current predefined course along the waterway direction.

Remark (*Choice of* θ). The parameter θ should be chosen within a certain range to ensure the collision-free motion of the ship towing system considering spatial limitation like the bank of waterway during maneuvering. There is a maximum value for θ, which is calculated by Hepworth (2021):

$$\theta_{max} = \arctan \frac{d_2(t)}{d_1(t)}$$

where $d_1(t)$ is the distance between two waypoints; $d_2(t)$ is the distance from the predefined path to the edge of the spatial boundaries. It can be seen that $d_1(t)$ and $d_2(t)$ are time-varying variables, because for different

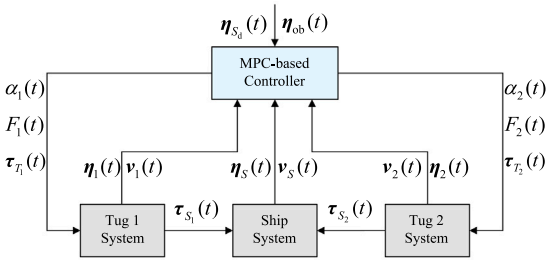

Fig. 6. Centralized control diagram.

two waypoints, $d_1(t)$ will be different; for different waterways, $d_2(t)$ will be different. Thus, the value of θ should satisfy: $0° < \theta < \theta_{\max}$.

3.2. MPC-based centralized optimization control problem

The ship reference system is the first stage of collision avoidance that focuses on complying with COLREGS. Considering the physical-connection constraints reducing the effectiveness of the steering operation and the low-speed conditions increasing the response time of the action, the second stage of collision avoidance is performed in the control system.

The challenge of the control problem for the physical-connected multi-vessel system are: (*a*) multiple control inputs need to be solved in each controller; (*b*) there are multiple constraints, such as the dynamics, the actuator saturation, and the configuration restriction, that the system should take into consideration; (*c*) the collision avoidance for such a low maneuverability system requires to take actions in advance. Thus, the model predictive control (MPC) strategy is applied in this work.

As shown in Fig. 6, at each time instant k, the MPC-based controller solves the following optimization problems to get the control inputs of the ship ($\boldsymbol{\tau}_S = \{F_1, F_2, \alpha_1, \alpha_2\}$) and the two tugs ($\boldsymbol{\tau}_{T_1} = \{\tau_{T_1 u}, \tau_{T_1 v}, \tau_{T_1 r}\}$, $\boldsymbol{\tau}_{T_2} = \{\tau_{T_2 u}, \tau_{T_2 v}, \tau_{T_2 r}\}$):

$$\min_{\boldsymbol{\tau}_S, \boldsymbol{\tau}_{T_1}, \boldsymbol{\tau}_{T_2}} \quad \sum_{h=1}^{H_P} J_S(k+h|k) + J_1(k+h|k) + J_2(k+h|k), \tag{12}$$

subject to (*i*) Ship and tugs dynamics, given by Eq. (15) and (16);

(*ii*) Ship and tugs actuator saturation, given by Eq. (17)–(21);

(*iii*) System configuration restriction, given by Eq. (4)–(6);

where H_P is the length of the prediction horizon; h is the hth time prediction step; $J_S(k+h|k)$, $J_1(k+h|k)$ and $J_2(k+h|k)$ are the prediction made at k about the cost function of the ship and two tugs at $k+h$, respectively.

The cost function of the three vessels is designed as:

$$\begin{aligned} J_*(k) &= w_{*1} \boldsymbol{e}_{\eta_*}^{\mathrm{T}}(k) \boldsymbol{e}_{\eta_*}(k) + w_{*2} \boldsymbol{v}_{*\mathrm{P}}^{\mathrm{T}}(k) \boldsymbol{v}_{*\mathrm{P}}(k) \\ &\quad + w_{*3} \sum_{j=1}^{n} \left(d_{*j}(k) - d_{*j_{\mathrm{d}}}\right)^{-2} \\ \boldsymbol{e}_{\eta_*}(k) &= \boldsymbol{\eta}_{*\mathrm{P}}(k) - \boldsymbol{\eta}_{*\mathrm{d}}(k), \end{aligned} \tag{13}$$

where $*$ can be S or i ($i = 1, 2$), w_{*1}, w_{*2} and w_{*3} are the weight coefficients (positive scalar); $\boldsymbol{e}_{\eta_*}(k) \in \mathbb{R}^3$ is the position error; $\boldsymbol{\eta}_{*\mathrm{d}}(k) \in \mathbb{R}^3$ is the desired position vector: for the ship, $\boldsymbol{\eta}_{S_{\mathrm{d}}}(k)$ is calculated by (10) and (11); for the tug i, $\boldsymbol{\eta}_{i_{\mathrm{d}}}(k)$ is calculated by (4). The term $\boldsymbol{\eta}_{*\mathrm{P}}(k) \in \mathbb{R}^3$ and $\boldsymbol{v}_{*\mathrm{P}}(k) \in \mathbb{R}^3$ are the predicted position and velocity; n is the number of obstacles. The term $d_{*j_{\mathrm{d}}}$ is the safe distance between the vessel and obstacle j, whose values are also calculated according to the attributes of the obstacle (see in Fig. 5):

$$d_{*j_{\mathrm{d}}} = \begin{cases} L + R_j + d_{\mathrm{S0}} & \text{for } j \text{ is circle obstacle} \\ 2(L + a_j + d_{\mathrm{S0}}) & \text{for } j \text{ is ellipse obstacle} \end{cases}, \tag{14}$$

where L is the length of the own-vessel; R_j is the radius of the circle obstacle j; a_j is the length of the long axis of the ellipse obstacle j; d_{S0} is the surplus distance (buffer) of the obstacles. Note that the safe distance $d_{*j_{\mathrm{d}}}$ is smaller than the detection distance d_{D}: $d_{*j_{\mathrm{d}}} < d_{\mathrm{D}}$.

It can be seen from (13) that the cost contains three parts. The first part is the position error, which is minimized to achieve path following. The second part is the velocity, whose role is to reduce the speed of the three vessels to make the motion of the system smooth. The third part is the distance error between the ship and the obstacles. It is a reciprocal quadratic term meaning that the further the ship from the safety distance of the obstacle, the less value of this term. This is the second stage of collision avoidance ensuring that the ship keeps away from the obstacles.

The vessel dynamics (the first constraint) is represented by the prediction model, which determines the predicted position and velocity of the ship and tug. They are calculated by discretizing the dynamic model in (1)–(3) with sample time T_s:

$$\begin{aligned} \boldsymbol{\eta}_{S_{\mathrm{P}}}(k+1) &= \boldsymbol{\eta}_{S_{\mathrm{P}}}(k) + \int_{kT_s}^{(k+1)T_s} \boldsymbol{R}\left(\psi_S(t)\right) \boldsymbol{v}_S(t) dt \\ \boldsymbol{v}_{S_{\mathrm{P}}}(k+1) &= \boldsymbol{v}_{S_{\mathrm{P}}}(k) + \int_{kT_s}^{(k+1)T_s} \boldsymbol{M}_S^{-1} \left[-\boldsymbol{C}_S\left(\boldsymbol{v}_S(t)\right) \boldsymbol{v}_S(t) \right. \\ &\quad \left. - \boldsymbol{D}_S \boldsymbol{v}_S(t) - \boldsymbol{B}\left(\alpha_1(t)\right) F_1(t) + \boldsymbol{B}\left(\alpha_2(t)\right) F_2(t) \right] dt, \end{aligned} \tag{15}$$

$$\begin{aligned} \boldsymbol{\eta}_{i_{\mathrm{P}}}(k+1) &= \boldsymbol{\eta}_{i_{\mathrm{P}}}(k) + \int_{kT_s}^{(k+1)T_s} \boldsymbol{R}\left(\psi_i(t)\right) \boldsymbol{v}_i(t) dt \\ \boldsymbol{v}_{i_{\mathrm{P}}}(k+1) &= \boldsymbol{v}_{i_{\mathrm{P}}}(k) + \int_{kT_s}^{(k+1)T_s} \boldsymbol{M}_i^{-1} \left[-\boldsymbol{C}_i\left(\boldsymbol{v}_i(t)\right) \boldsymbol{v}_i(t) \right. \\ &\quad \left. - \boldsymbol{D}_i \boldsymbol{v}_i(t) + \boldsymbol{B}_i\left(\beta_i(t)\right) F_i(t) + \boldsymbol{\tau}_{T_i}(t) \right] dt. \end{aligned} \tag{16}$$

The actuator saturation (the second constraint) stems from the physical laws and maritime practice (Hensen, 2003). For all k over the prediction horizon and $i = 1, 2$:

$$-\alpha_{i\max} \le \alpha_i(k) < \alpha_{i\max} \tag{17}$$

$$0 \le F_i(k) \le F_{i\max} \tag{18}$$

$$-\boldsymbol{\tau}_{i\max} \le \boldsymbol{\tau}_i(k) \le \boldsymbol{\tau}_{i\max} \tag{19}$$

$$\left|\dot{\alpha}_i(k)\right| \le \bar{\alpha}_i \tag{20}$$

$$\left|\dot{F}_i(k)\right| \le \bar{F}_i, \tag{21}$$

where $\alpha_{i\max}$ is the maximum value of towing angle; $F_{i\max}$ is the maximum value of towing force that the two towing lines withstand; $\boldsymbol{\tau}_{i\max}$ is the maximum value of the thruster forces and moment; $\bar{\alpha}_i$ and $\bar{F}_i$ are the maximum change rate value of towing angle and force, respectively.

The configuration restriction (the third constraint) is to satisfy the configuration of the towing system to keep the desired geometrical relationship between the ship and tugs (see Fig. 1).

From the implementation point of view, the Ship Reference System runs at the same sampling rate as the control system, while the distance calculation in the Ship Reference System is sampled from variables that change continuously between samples. The selection of sampling rate is not the focus of this paper. Interested readers may refer to the literature (Binder et al., 2019).

3.3. ADMM-based distributed MPC scheme

Although the centralized control scheme in Section 3.2 can solve the optimization problem, if the number of tugboats increases, the number of control inputs and constraints will also increase, and the structure inside the controller will also change. To improve the proposed method applicably, it is necessary to divide such a large global optimization problem into several small local optimization problems. Thus, the distributed control scheme is proposed, and the distributed

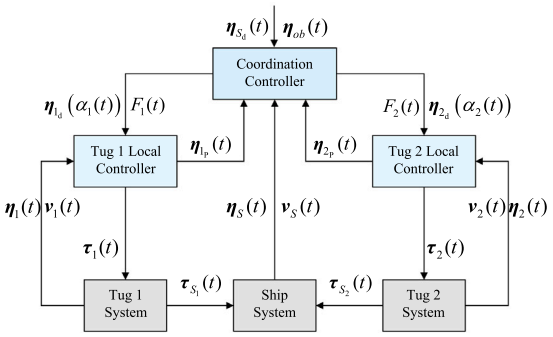

Fig. 7. System control diagram.

architecture is achieved by using the Altering Direction Method of Multipliers (ADMM).

The ADMM is a widely used algorithm well suited for distributed optimization, especially for consensus problems (Ren et al., 2005). The idea of the ADMM is to blend the dual ascent optimization approach with the augmented Lagrange multiplier method (Stephen et al., 2010), which is characterized by superior decomposability and convergence properties. For our case, the MPC-based controller in Fig. 6 can be divided into three sub-controllers according to their functions: Coordination controller, Tug 1 local controller, and Tug 2 local controller.

As seen in Fig. 7, the coordination controller, located on the ship, uses the information of ship desired position and heading $\boldsymbol{\eta}_{S_\mathrm{d}}(t)$, obstacle position and heading $\boldsymbol{\eta}_{\mathrm{ob}}(t)$, and the current states of the ship $\boldsymbol{\eta}_S(t)$, $\boldsymbol{\nu}_S(t)$ to compute the towing forces $F_i(t)$ and the desired tug trajectory reference $\boldsymbol{\eta}_{i_\mathrm{d}}(t)$ which is a function of towing angles $\alpha_i(t)$. The tug local controller, located on the tug, uses the calculated towing force, tug trajectory reference, and the current states of tugs $\boldsymbol{\eta}_i(t)$, $\boldsymbol{\nu}_i(t)$ to first calculate the predicted position $\boldsymbol{\eta}_{i_\mathrm{P}}(t)$, and share this information with the coordination controller to reach a consensus between the predicted position and the tug reference trajectory ($\boldsymbol{\eta}_{i_\mathrm{P}}(t) = \boldsymbol{\eta}_{i_\mathrm{d}}(t)$). Then, the coordination controller updates the towing forces and angles. When the consensus is achieved, the tug local controller outputs the thruster forces and moment $\boldsymbol{\tau}_i(t)$ to the tug system.

Based on the above analysis, the augmented Lagrangian form for our problem at time instant k can be formulated as:

$$\begin{aligned} L_p\big(\boldsymbol{\tau}_S(k), \boldsymbol{\tau}_{T_i}(k), \lambda_i(k)\big) = J_S\big(\boldsymbol{\tau}_S(k)\big) + \sum_{i=1}^{2} \Big(J_i\big(\boldsymbol{\tau}_{T_i}(k)\big) \\ + \lambda_i^{\mathrm{T}}(k)[\boldsymbol{\eta}_{i_\mathrm{P}}(k) - \boldsymbol{\eta}_{i_\mathrm{d}}(k)] + \\ (\rho/2)\left\|\boldsymbol{\eta}_{i_\mathrm{P}}(k) - \boldsymbol{\eta}_{i_\mathrm{d}}(k)\right\|_2^2 \Big), \end{aligned} \tag{22}$$

where $\lambda_i(k)$ is the Lagrange multiplier or dual variable, and ρ is the penalty parameter. Variable $\boldsymbol{\eta}_{i_\mathrm{d}}(k)$ is calculated by (4), which is a function of the towing angle ($\alpha_i(k)$) and the ship predicted heading ($\psi_{S_\mathrm{P}}(k)$). The variable $\alpha_i(k)$ is a part of the $\boldsymbol{\tau}_S(k)$, and $\psi_{S_\mathrm{P}}(k)$ can be calculated by ship dynamics (15). Thus, $\boldsymbol{\eta}_{i_\mathrm{d}}(k)$ can be expressed as a function of $\boldsymbol{\tau}_S(k)$:

$$\boldsymbol{\eta}_{i_\mathrm{d}}(k) = f_i\big(\boldsymbol{\tau}_S(k)\big). \tag{23}$$

Similarly, $\boldsymbol{\eta}_{i_\mathrm{P}}(k)$ can be calculated by tug dynamics (16), so it is a function of $\boldsymbol{\tau}_{T_i}(k)$:

$$\boldsymbol{\eta}_{i_\mathrm{P}}(k) = g_i\big(\boldsymbol{\tau}_{T_i}(k)\big). \tag{24}$$

Based on (22), (23), and (24), the ADMM form of the iterations are formulated as:

$$\begin{aligned} \boldsymbol{\tau}_{T_i}^s(k) := \underset{\boldsymbol{\tau}_{T_i}(k)}{\arg\min} \Big(J_i\big(\boldsymbol{\tau}_{T_i}(k)\big) + \lambda_i^{s-1}(k)^{\mathrm{T}} \Big[g_i\big(\boldsymbol{\tau}_{T_i}(k)\big) - \\ f_i\big(\boldsymbol{\tau}_S^{s-1}(k)\big) \Big] + (\rho/2)\left\|g_i\big(\boldsymbol{\tau}_{T_i}(k)\big) - f_i\big(\boldsymbol{\tau}_S^{s-1}(k)\big)\right\|_2^2 \Big), \end{aligned} \tag{25}$$

Algorithm 1 - ADMM-based Distributed Control

Input: Obstacle position $\eta_{ob}(t)$; Desired ship position $\eta_{S_\mathrm{d}}(t)$; Current ship position and velocity $\eta_S(t)$, $\nu_S(t)$; Current tug position and velocity $\eta_i(t)$, $\nu_S(t)$.

1: *For* $s = 1 : S$
2: **Step 1:** At the lower level, each tug local controller calculates the thruster forces and moment of the tug $\tau_{T_i}^s(k)$ according to (25), and sends the results to the coordination controller;
3: **Step 2:** At the higher level, the coordination controller computes the manipulation forces and moment for the ship $\tau_S^s(k)$ according to (26);
4: **Step 3:** In both tug and coordination controllers, update the Lagrange multiplier $\lambda_i^s(k)$ according to (27);
5: **Step 4:** In coordination controller, update the primal $\varepsilon_{\mathrm{pri},i}^s(k)$ and dual $\varepsilon_{\mathrm{dual},i}^s(k)$ tolerances according to (29), and checks the primal $\boldsymbol{R}_{\mathrm{pri},i}^s(k)$ and dual $\boldsymbol{R}_{\mathrm{dual},i}^s(k)$ residuals whether they meet the termination criteria according to (28);
6: **Step 5:** If (28) is not satisfied, then repeat the above steps; otherwise, jump out of the iteration.
7: *End*

Output: Thruster forces and moment of the tug $\tau_{T_i}^s(k)$; Manipulation forces and moment for the ship $\tau_S^s(k)$.

$$\begin{aligned} \boldsymbol{\tau}_S^s(k) := \underset{\boldsymbol{\tau}_S(k)}{\arg\min} \Big(J_S\big(\boldsymbol{\tau}_S(k)\big) + \sum_{i=1}^{2} \Big(-\lambda_i^{s-1}(k)^{\mathrm{T}} f_i\big(\boldsymbol{\tau}_S(k)\big) \\ + (\rho/2)\left\|g_i\big(\boldsymbol{\tau}_{T_i}^s(k)\big) - f_i\big(\boldsymbol{\tau}_S(k)\big)\right\|_2^2 \Big) \Big), \end{aligned} \tag{26}$$

$$\lambda_i^s(k) := \lambda_i^{s-1}(k) + \rho_i\Big(g_i\big(\boldsymbol{\tau}_{T_i}^s(k)\big) - f_i\big(\boldsymbol{\tau}_S^s(k)\big)\Big), \tag{27}$$

where s is the iteration with $s \in \{1, 2, \cdots S\}$, S is the maximum iteration; $\cdot^s$ stands for the corresponding variable at the sth iteration.

The termination criterion for the iterations is provided according to the following conditions:

$$\begin{aligned} \left\|\boldsymbol{R}_{\mathrm{pri},i}^s(k)\right\|_2 = \left\|g_i\big(\boldsymbol{\tau}_{T_i}^s(k)\big) - f_i\big(\boldsymbol{\tau}_S^s(k)\big)\right\|_2 \le \varepsilon_{\mathrm{pri},i}^s(k), \\ \left\|\boldsymbol{R}_{\mathrm{dual},i}^s(k)\right\|_2 = \left\|f_i\big(\boldsymbol{\tau}_S^s(k)\big) - f_i\big(\boldsymbol{\tau}_S^{s-1}(k)\big)\right\|_2 \le \varepsilon_{\mathrm{dual},i}^s(k), \end{aligned} \tag{28}$$

where $\boldsymbol{R}_{\mathrm{pri},i}^s$ and $\boldsymbol{R}_{\mathrm{dual},i}^s$ are the primal and dual residual at iteration s; $\varepsilon_{\mathrm{pri},i}^s > 0$ and $\varepsilon_{\mathrm{dual},i}^s > 0$ are feasibility tolerances, determined by

$$\begin{aligned} \varepsilon_{\mathrm{pri},i}^s(k) = \sqrt{n_s}\varepsilon^{\mathrm{abs}} + \varepsilon^{\mathrm{rel}} \max\Big\{ \left\|g_i\big(\boldsymbol{\tau}_{T_i}^s(k)\big)\right\|_2, \\ \left\|f_i\big(\boldsymbol{\tau}_S^s(k)\big)\right\|_2 \Big\}, \\ \varepsilon_{\mathrm{dual},i}^s(k) = \sqrt{n_s}\varepsilon^{\mathrm{abs}} + \varepsilon^{\mathrm{rel}}\left\|\lambda_i^s(k)\right\|_2, \end{aligned} \tag{29}$$

where n_s is the size of the variable $\boldsymbol{\tau}_{T_i}$; $\varepsilon^{\mathrm{abs}} > 0$ and $\varepsilon^{\mathrm{rel}} > 0$ are the absolute and relative tolerance, respectively.

Overall, the ADMM-based distributed control scheme for a physically interconnected multi-ASV system performing a ship towing process is summarized in the **Algorithm 1**.

4. Simulation experiment and result analysis

Simulation results are presented in this section to show the performance of the proposed method applied to a ship-towing system of small scale vessels.

4.1. Simulation setup

Two small-scale vessel models are used in the simulations: The "*TitoNeri*" developed by TU Delft (Skjetne et al., 2004), and the

Table 2
Parameters of the towing system.

Physical system	Tug 1 (after)	Towline 1	Ship	Towline 2	Tug 2 (forward)
Model of the vessel	*TitoNeri*		*CyberShip II*		*TitoNeri*
Length of the vessel	0.97 m		1.225 m		0.97 m
Width of the vessel	0.30 m		0.29 m		0.30 m
Mass of the vessel	16.9 kg		23.8 kg		16.9 kg
Desired elongation of the towline		$l_{\text{tow}_1} = 1$ m		$l_{\text{tow}_2} = 1$ m	
Distance from the ship center of gravity			$l_1 = 0.67$ m		
			$l_2 = 0.585$ m		
Distance from the tug center of gravity	$l_{\text{T}_1} = 0.5$ m				$l_{\text{T}_2} = 0.5$ m
Maximum values of the towing angles		$\alpha_{1\max} = 30°$		$\alpha_{2\max} = 30°$	
Maximum values of the towing forces		$F_{1\max} = 3$ N		$F_{2\max} = 3$ N	
Maximum values of the thruster forces	$\tau_{1\max} = 10$ N				$\tau_{2\max} = 10$ N

Table 3
Parameters of the control system.

Altering angle	$\theta = 15°$
Sampling time	$T_s = 1$ s
Prediction horizon	$H_P = 3$
Weight coefficient in cost function J_S	$w_{S_1} = 1,\ w_{S_2} = 75,\ w_{S_3} = 1$
Weight coefficient in cost function J_i	$w_{i_1} = 1,\ w_{i_2} = 6,\ w_{i_3} = 1,\ (i = 1, 2)$
Absolute and relative tolerance in ADMM	$\varepsilon^{\text{abs}} = 0.001,\ \varepsilon^{\text{rel}} = 0.001$
Maximum rate of the change of towing angles	$\bar{\alpha}_1 = 5°/\text{s},\ \bar{\alpha}_2 = 5°/\text{s}$
Maximum rate of the change of towing forces	$\bar{F}_1 = 0.3\,\text{N/s},\ \bar{F}_2 = 0.3\,\text{N/s}$

Table 4
Position and heading[a] of the predefined waypoint.

$\eta_{\text{W}_{\text{P1}}} = [-6.3 \quad 14 \quad 101.3°]^{\text{T}}$	$\eta_{\text{W}_{\text{P5}}} = [-7.7 \quad 21 \quad 101.3°]^{\text{T}}$
$\eta_{\text{W}_{\text{P2}}} = [-9.1 \quad 28 \quad 101.3°]^{\text{T}}$	$\eta_{\text{W}_{\text{P6}}} = [-10.7 \quad 36 \quad 101.3°]^{\text{T}}$
$\eta_{\text{W}_{\text{P3}}} = [-15 \quad 40 \quad 180°]^{\text{T}}$	$\eta_{\text{W}_{\text{P7}}} = [-22 \quad 40 \quad 180°]^{\text{T}}$
$\eta_{\text{W}_{\text{P4}}} = [-29 \quad 40 \quad 180°]^{\text{T}}$	$\eta_{\text{W}_{\text{P8}}} = [-36 \quad 40 \quad 180°]^{\text{T}}$

[a]The heading of the waypoint is defined along the direction of the waterway.

"*CyberShip II*" developed by NTNU (Haseltalab and Negenborn, 2019). The parameters of the towing system are shown in Table 2, the parameters of the control system are given in Table 3.

The objective is to cooperatively control two autonomous tugboats that safely manipulate the ship from the origin ($\eta_{\text{W}_{\text{PO}}} = [-4.9 \quad 7 \quad 101.3°]^{\text{T}}$) to the destination ($\eta_{\text{W}_{\text{PD}}} = [-43 \quad 40 \quad 180°]^{\text{T}}$). Between the origin and destination, there are eight predefined waypoints (the values are shown in Table 4), which should be followed when there are no obstacles. There are three static obstacles (a, b, c) and three dynamic obstacles (A, B, C) during the towing process, whose information is shown in Table 5.

4.2. Results and discussion

4.2.1. Ship towing process

The towing process is shown in Fig. 8, which is represented by ten sampled states of the towing system. From $t_1 = 0$ s to $t_2 = 100$ s, the control objective is path following. The two tugs manipulate the ship from the origin (W_{PO}) to the first waypoint (W_{P1}). From $t_2 = 100$ s to $t_3 = 190$ s, the system encounters the first avoidance scenario, crossing. In this case, the towing system has to avoid the first moving vessel and stay away from the dangerous area a. The trajectories indicate that the system executes starboard (right) side steering operation to bypass the moving vessel (satisfy the COLREGS), and all the trajectories did not cross over the dangerous area a. After avoiding the moving vessel, the system returns to the predefined path to continue to follow the rest of the waypoints, whose process is from $t_3 = 190$ s to $t_4 = 300$ s. From the trajectories, it is clear that the three vessels stay away from the dangerous area b and return to the third waypoint (W_{P3}).

From $t_4 = 300$ s to $t_5 = 405$ s, the towing system follows the predefined path to the fourth waypoint (W_{P4}). From $t_5 = 405$ s to $t_6 = 495$ s, the towing system performs a starboard steering operation and comes across two obstacles, facing the avoidance scenario that contains both crossing and head-on. The trajectories show that the towing system carries out a heavy starboard steering to make the three vessels avoid the second moving obstacle, which makes the trajectory of the ship biases to the right-hand side of the fifth waypoint (W_{P5}), satisfying the COLREGS. Besides, all three vessels stay away from the dangerous areas c in the steering process, reflecting that the control

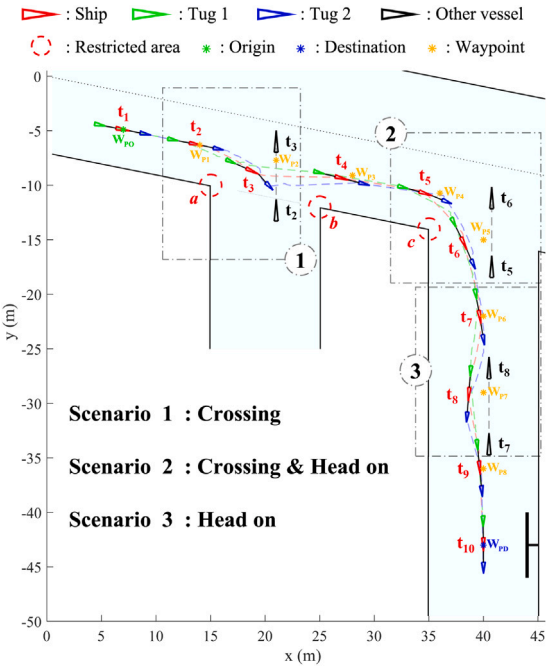

Fig. 8. Towing process in congested water traffic environment: The black "T" shape stands for a pier, the tip of the marker representing a ship corresponds to the bow.

Table 5
Information of the obstacles.

Obstacle	Length (m)	Width (m)	Course (degree)	Speed (m/s)	Position (initial)
Static *a*	1	1	–	0	(−10,15)
Static *b*	1	1	–	0	(−12,25)
Static *c*	1	1	–	0	(−14,35)
Dynamic *A*	1.48	0.48	0	0.07	(−19,21)
Dynamic *B*	1.48	0.48	0	0.07	(−22,40.75)
Dynamic *C*	1.48	0.48	0	0.07	(−38,40.5)

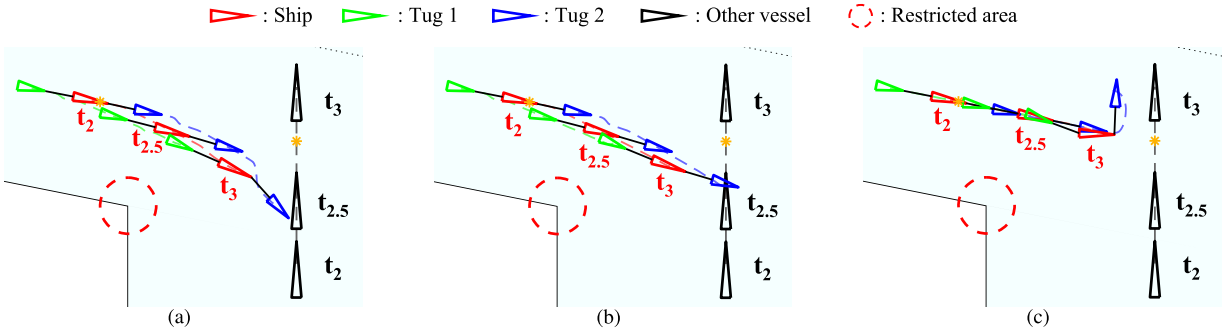

Fig. 9. Three collision avoidance schemes are applied to deal with avoidance scenario 1 (crossing) during t_2 = 100 s to t_3 = 190 s ($t_{2.5}$ = 135 s): (a) Scheme I; (b) Scheme II; (c) Scheme III.

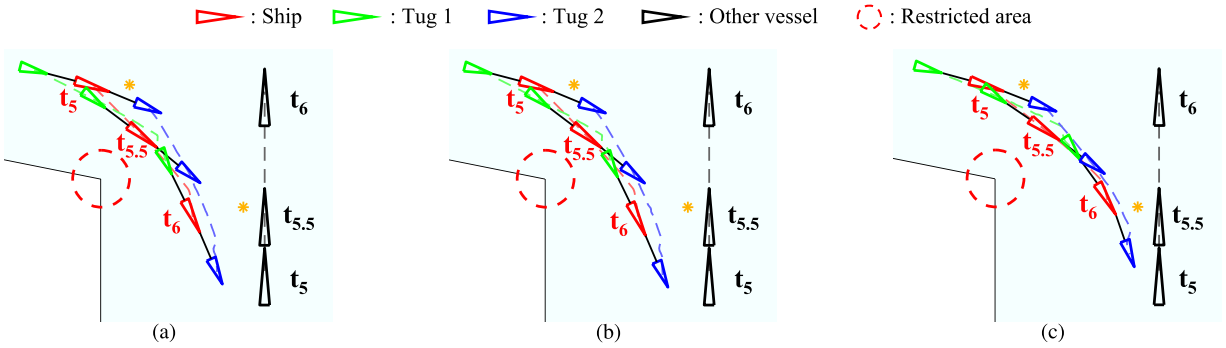

Fig. 10. Three collision avoidance schemes are applied to deal with avoidance scenario 2 (crossing & heading) during t_5 = 405 s to t_6 = 495 s ($t_{5.5}$ = 435 s): (a) Scheme I; (b) Scheme II; (c) Scheme III.

scheme can make sure the towing system navigate in such a narrow waterway condition.

From t_6 = 485 s to t_7 = 590 s, the towing system again returns to the planned path to follow the sixth waypoint W_{P6}. From t_7 = 590 s to t_8 = 690 s, the system encounters the third avoidance scenario. The course of the third moving obstacle is right toward the seventh waypoint (W_{P7}), so this is the head-on scenario. The steering trajectories are illustrated that the towing system takes actions of starboard steering to pass on the port side of the third moving obstacle (satisfy the COLREGS). The period from t_8 = 690 s to t_9 = 785 s is the third returning process, aiming at the eighth waypoint (W_{P8}). The last period from t_9 = 785 s to t_{10} = 969 s is the stabilizing process that the two tugs stop the ship at the destination (W_{PD}) with desired heading.

Fig. 8 shows that the proposed cooperative control algorithm can make the two autonomous tugs manipulate a ship to the destination with the desired heading without colliding the static and dynamic obstacles.

4.2.2. Avoidance scheme comparison

In order to show the necessity of the two stages of obstacle avoidance, three different collision avoidance schemes are compared: Scheme I is the proposed scheme, combining the waypoint altering system (stage 1) and the distance cost function (stage 2); Scheme II is

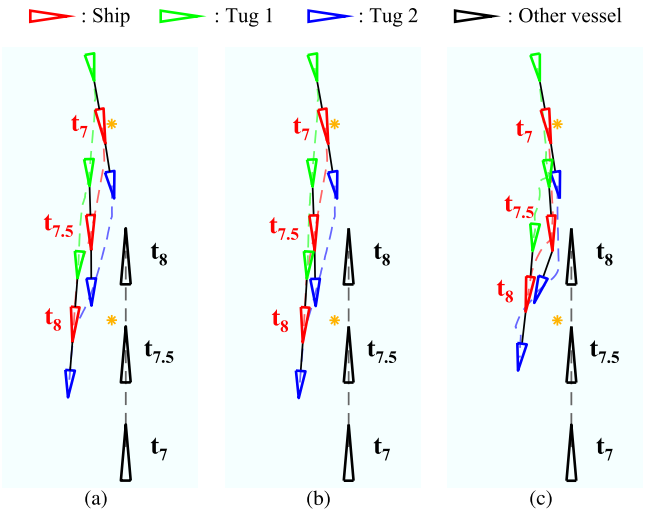

Fig. 11. Three collision avoidance schemes are applied to deal with avoidance scenario 3 (heading) during t_7 = 590 s to t_8 = 690 s ($t_{7.5}$ = 640 s): (a) Scheme I; (b) Scheme II; (c) Scheme III.

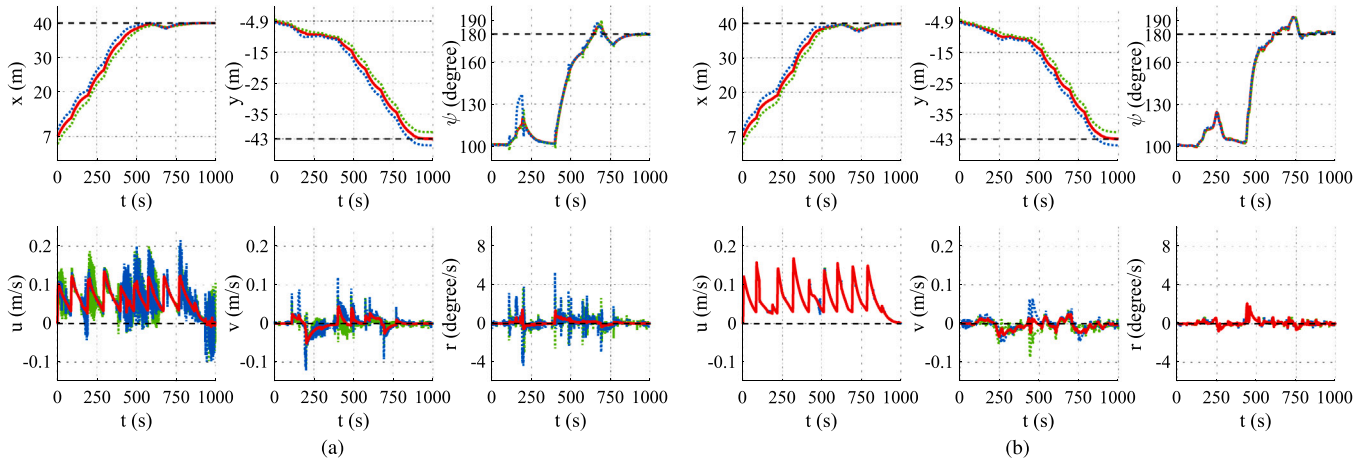

Fig. 12. Six states (position (x, y), heading ψ and velocities u, v, r) of the ship (red bold line) and two tugs (green dashed line stands for Tug 1 and blue dotted line for Tug 2): (a) The distributed control architecture; (b) The centralized control architecture. (For interpretation of the references to color in this figure legend, the reader is referred to the web version of this article.)

the one that only uses the waypoint altering system (stage 1); Scheme III is the one that only uses the distance cost function (stage 2). The collision avoidance process of the three schemes applied to deal with the three different scenarios in Fig. 8 is shown in Fig. 9–Fig. 11.

For scenario 1 (Fig. 9), scheme III makes the towing system steer the port side to avoid the obstacle, this operation violates the COLREGS rules. Scheme I and II comply with the rules making the towing system take action of starboard steering, while the scheme I has greater steering during $t_{2.5} = 135$ s and $t_3 = 190$ s to make sure the towing system stays away from the obstacle. For scenario 2 (Fig. 10) and scenario 3 (Fig. 11), the three schemes have similar collision resolutions that successfully bypass the obstacle and comply with the COLREGS rules. Compared to the other two schemes, the response time of the collision avoidance in scheme III is longer, which makes the distance between the vessels in the towing system and the obstacles smaller at the beginning. To verify this, the performance indicator about the minimum distance between the three vessels in the towing system and the obstacles are proposed and calculated as follows:

$$D_{\mathrm{ob}_j*} = \min\ d_{\mathrm{ob}_j*}/L_* \tag{30}$$

where d_{ob_j*} is distance between the vessel in the towing system (* stands for S (for ship) and i (for tugboat)) and the obstacle j. For static obstacles, d_{ob_j*} is calculated by (9); for dynamic obstacles, d_{ob_j*} is calculated from the vessel's position to the central of gravity of the obstacle. The term L_* is the length of the vessel. Note that *i*) (30) normalizes the minimum distance by eliminating the effect of the length of the vessel; *ii*) the larger the D_{ob_j*}, the safer the vessel.

The normalized minimum distance between the vessels in the towing system and the obstacles by using three avoidance schemes in three scenarios are shown in Table 6. In scenario 1, as the greater steering observed in Fig. 9(a), the values for three vessels by using scheme I are larger than scheme II. The COLREGS-violated steering in scheme III makes the value of tug 1 ($D_{\mathrm{ob}_1 1}$) a little larger than that in the scheme I, but the other two values are smaller (even than scheme II). In scenario 2, the results in schemes I and II are similar, larger than scheme III. In scenario 3, the superiority in scheme I is more obvious, and the result in scheme III is still the worst because of the longer response time.

Overall, the collision avoidance scheme II has the largest normalized minimum distance between the vessels and obstacles in all three scenarios, revealing that the proposed control scheme is the safest in dealing with obstacles, and combining two collision avoidance stages (the waypoint altering system and the distance cost function) is rational. The total computation time of the proposed method is 2147 s (the whole simulation time is 1000 s). For each collision avoidance scenario, the average computation time is the same. Thus, for every one-second simulation process, the proposed method spends 2 s to calculate the desired control inputs. The reason for this computation time is that the model of the towing system is nonlinear, while the iterations of the ADMM in this paper are ten to thirty. So the repeating nonlinear computation requires a lot of time.

4.2.3. Control architecture comparison

In this subsection, we compare the results of the centralized and distributed control architecture applied under the above simulation conditions. The time-varying states of the ship and two tugs using the two control architectures are shown in Fig. 12. It can be seen from the first row of the figure that in both architectures the ship achieves its desired position and heading eventually, and the varying of the values in each state are similar. The differences are shown in the velocity of the second row. For the ship surge velocity (in red bold line in u), the changes in two architectures show similar results: Saw-shape fluctuations. The nine "sawtooths" indicate the process of waypoint following (eight waypoints and a destination point). The reason for the "sawtooth" is the change in position error. In each waypoint following process, the value of ship position error is maximum at the beginning, dominating in (13). The coordination controller at the moment focuses on reducing this error and then increases the ship surge speed to a large value. As the ship approaches the waypoint, the position error becomes small, the proportion of velocity part increases. The objective of the coordination controller gradually switches to velocities, the ship surge speed starts decreasing.

However, the changes in the two tugs' surge velocity (green and blue dashed line) in the two architectures are much different. In Fig. 12(a), these results show much more fluctuation compared to the ship; but in Fig. 12(b), these results are similar to the ship. This can be explained by the fact that the centralized control method (Du et al., 2021b) is to solve a large global optimization problem concerning all the vessels, so the change of surge velocity of the tugs will be consistent with the ship as much as possible; while the distributed control method is to separately solve the local optimization problems for each vessel, leading to different surge of the tugs and ship. As the power of the ship is provided by the tugs, the surge velocity of the tugs have more frequent changes in the distributed control. The values of the sway (v) and yaw (r) velocity show large changes during the collision avoidance operations in both control architectures, but the magnitude and frequency of the changes in the distributed control are larger than that of the centralized.

The towing angles and forces are shown in Fig. 13, and their change rate are shown in Fig. 14. It is observed that the values of all the variables are within the boundary in both architectures, which satisfies

Table 6
Normalized minimum distance between the vessels in the towing system and the obstacles.

Collision avoidance scheme	Scenario 1 (Crossing)	Scenario 2 (Crossing & Head-on)	Scenario 3 (Head-on)	COLREGS compliance	
I	$D_{ob_1}S = 2.45$ $D_{ob_1}1 = 4.31$ $D_{ob_1}2 = 1.53$	$D_{ob_2}S = 2.65$ $D_{ob_2}1 = 3.97$ $D_{ob_2}2 = 2.41$	$D_{ob_3}S = 1.43$ $D_{ob_3}1 = 1.70$ $D_{ob_3}2 = 1.73$	Scenario 1 Scenario 2 Scenario 3	✓ ✓ ✓
II	$D_{ob_1}S = 2.30$ $D_{ob_1}1 = 4.17$ $D_{ob_1}2 = 1.36$	$D_{ob_2}S = 2.62$ $D_{ob_2}1 = 3.95$ $D_{ob_2}2 = 2.34$	$D_{ob_3}S = 1.23$ $D_{ob_3}1 = 1.50$ $D_{ob_3}2 = 1.45$	Scenario 1 Scenario 2 Scenario 3	✓ ✓ ✓
III	$D_{ob_1}S = 1.93$ $D_{ob_1}1 = 4.40$ $D_{ob_1}2 = 1.44$	$D_{ob_2}S = 2.19$ $D_{ob_2}1 = 3.54$ $D_{ob_2}2 = 1.78$	$D_{ob_3}S = 1.13$ $D_{ob_3}1 = 1.30$ $D_{ob_3}2 = 1.67$	Scenario 1 Scenario 2 Scenario 3	× ✓ ✓

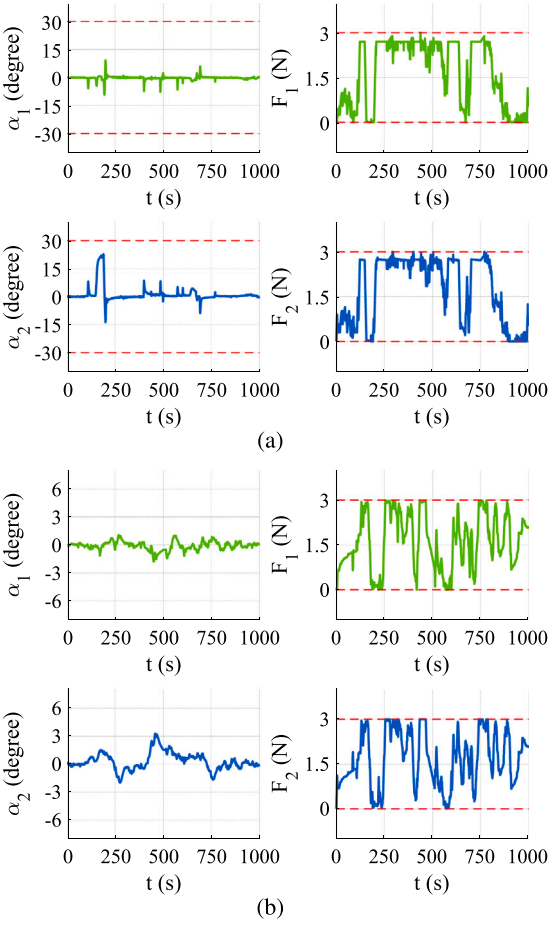

Fig. 13. Towing angles and forces: (a) The distributed control architecture; (b) The centralized control architecture.

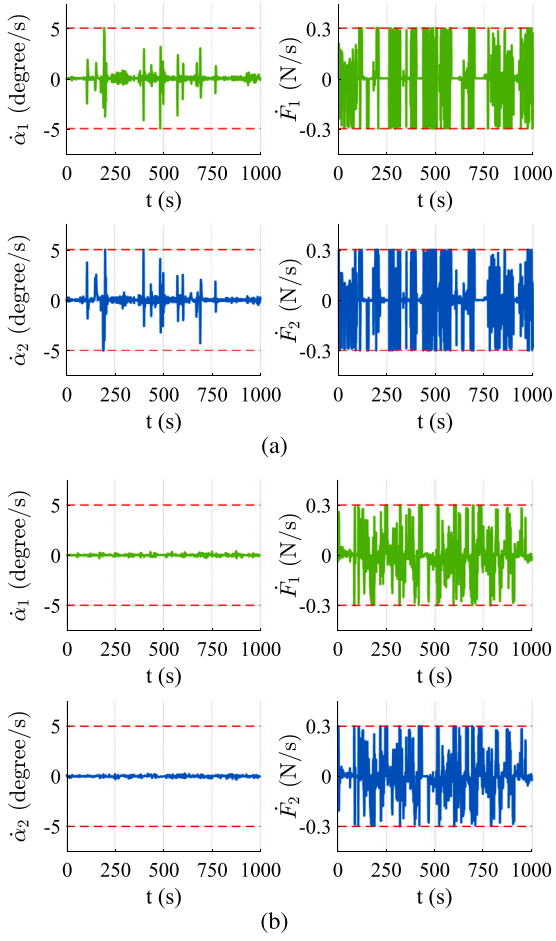

Fig. 14. Change rate of the towing angles and forces: (a) The distributed control architecture; (b) The centralized control architecture.

the saturation constraints. For the two towing angles, *i*) their magnitude and change rate in distributed control is larger than that in centralized control; *ii*) the values of the forward angle (α_2) is larger than the after angle (α_1). The reason for the first observation is that the motion of tugs is consistent with the ship as much as possible in centralized control making the magnitude and change of the towing angle small. The second observation results from the different functions of the two tugs. The forward tug is to change the ship course and increase the speed, the after tug is to stabilize the ship and reduce the speed. So the forward towing angle has larger change. For the two towing forces, the duration of maximum value and the frequency of change in distributed control is larger than that in centralized control, because compared to global optimization problem each separated local optimization problem makes each controller focus more on its own control objective, which results in the continuous high value of the control inputs.

The performance of the two control architectures is quantified and compared in Table 7. For the collision avoidance performance (columns 2 to 4), the normalized minimum distance between the vessels in the towing system and the obstacles using the centralized control method is larger than those using distributed control in scenarios 1 (crossing) and 3 (head-on). While in the more complex scenario 2 (crossing & head-on), the corresponding values using centralized control are smaller than those using distributed control. This indicates that the distributed control is better to deal with complex collision avoidance problems.

The control performance is characterized by settling time and maximum towline elongation error. The settling time is defined that the

Table 7
Avoidance and control performance of the distributed and centralized control architecture.

Control architecture	Normalized minimum distance to the obstacles			Settling time	Maximum towline elongation error	
	Scenario 1 (Crossing)	Scenario 2 (Crossing & Head-on)	Scenario 3 (Head-on)		Towline 1	Towline 2
Distributed	$D_{ob_1S} = 2.45$ $D_{ob_11} = 4.31$ $D_{ob_12} = 1.53$	$D_{ob_2S} = 2.65$ $D_{ob_21} = 3.97$ $D_{ob_22} = 2.41$	$D_{ob_3S} = 1.43$ $D_{ob_31} = 1.70$ $D_{ob_32} = 1.73$	$T = 968$ s	$\Delta l_{tow_1} = 5.79\%$	$\Delta l_{tow_2} = 6.33\%$
Centralized	$D_{ob_1S} = 2.79$ $D_{ob_11} = 5.25$ $D_{ob_12} = 1.74$	$D_{ob_2S} = 2.20$ $D_{ob_21} = 3.08$ $D_{ob_22} = 1.92$	$D_{ob_3S} = 1.59$ $D_{ob_31} = 2.12$ $D_{ob_32} = 1.73$	$T = 985$ s	$\Delta l_{tow_1} = 5.15\%$	$\Delta l_{tow_2} = 5.32\%$

states of the ship satisfy the following conditions: (*i*) The distance from the current position to the desired position is less than half length of the ship; (*ii*) The difference between the actual and desired heading is less than 3 degrees; (*iii*) The surge and sway velocities are less than 0.01 m/s, the yaw velocity is less then 0.01 rad/s. The towline elongation error is calculated by $e_{l_{tow}i} = |l_{tow_i} - l_{el_i}(t)| \ / \ l_{tow_i}$, where $l_{el_i}(t)$ is the actual elongation of the towline i.

As seen the columns 5 to 7 in Table 7, the settling time applying the centralized control is a bit larger than the settling time of distributed control, but the maximum towline elongation error by centralized control is smaller than distributed one. The difference in settling time may come from the different total traveling distance of the manipulated ship: 63.57 m for the centralized, 62.69 m for the distributed. The ship trajectory of the two control architectures are shown in Fig. 15. It can be seen that the extra traveling parts happen in the avoidance process. Because of the lower tug maneuverability in centralized control, the collision avoidance and waypoint returning operations are time-consuming. On the other hand, the better maneuverability of the tugs by distributed control makes the towing angles and forces more frequently changing, resulting in the larger value of the maximum towline elongation error. This indicator revels the smoothness of the towing process, but it can be seen that the difference of this indicator between the two control architectures is not much.

Overall, although there are some detailed differences (the tugs states, towing angles and forces) between the distributed and centralized control, the control objective achievements, the control constraints satisfaction, and the collision avoidance and control performance are similar. For the settling time and total traveling distance, the distributed control outperforms. This reveals that in our application, the results of the distributed local optimization problem are quite close to the results of the centralized global optimization problem.

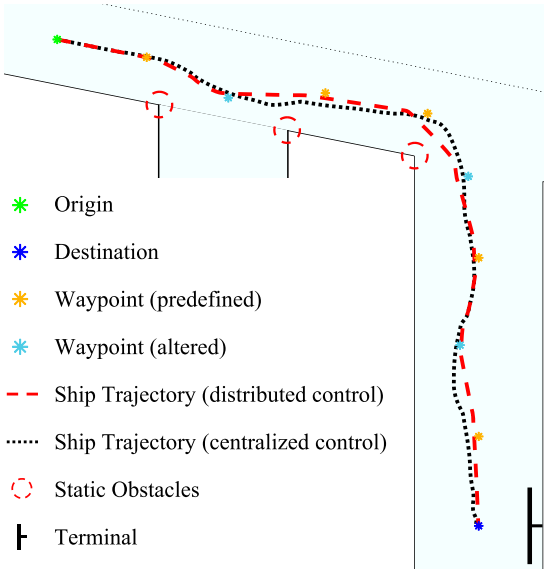

Fig. 15. Trajectory of the manipulated ship by two control architectures.

5. Conclusions and future research

This work focuses on distributed control of a multi-vessel ship-towing system for obstacle avoidance. We propose a COLREGS compliant ADMM-based MPC approach to coordinate multiple autonomous vessels, dealing with obstacle avoidance in the towing process in restricted waters. Such a complex problem is solved by cooperatively dealing with three sub-optimization problems. The coordinating MPC controller uses ship reference determined with the COLREGS-complied waypoint altering system to optimize the towing forces and angles for the ship waypoint following and obstacle avoidance problems. The tug local MPC controller on the tugboat utilizes the computed towing force and the tug reference calculated by the tug–ship configuration system to optimize the thruster forces and moment for the tug online trajectory tracking and obstacle avoidance problems. The consensus problem between the ship and tugs is solved by using the ADMM algorithm to find the optimal Lagrange Multipliers (dual variables) to achieve the distributed control architecture. Simulation experiments indicate that the proposed distributed control approach can avoid static and dynamic obstacles in restricted waterways for a physically interconnected multi-vessel system in the towing process, making the collision avoidance COLREGS compliant.

In future research, dealing with multiple target vessels in collision avoidance will be investigated to enhance the applicability of the proposed method. Implementation issues will be researched in the future when applying this method to small- and large-scale vessels. These issues will evolve reducing the computation time of the resolution to the optimization problem, and finding a proper choice of sampling time and horizon to guarantee that the constraints are not violated (Veksler et al., 2016).

CRediT authorship contribution statement

Zhe Du: Conceptualization, Methodology, Software, Investigation, Writing – original draft, Visualization. **Rudy R. Negenborn:** Conceptualization, Writing – review & editing, Supervision, Project administration. **Vasso Reppa:** Conceptualization, Writing – review & editing, Supervision, Project administration.

Declaration of competing interest

The authors declare that they have no known competing financial interests or personal relationships that could have appeared to influence the work reported in this paper.

Acknowledgment

This research is supported by the China Scholarship Council under Grant 201806950080, the Researchlab Autonomous Shipping (RAS) of Delft University of Technology, The Netherlands, and the INTERREG North Sea Region Grant "AVATAR" funded by the European Regional Development Fund.

References

Ahmed, Y.A., Hannan, M.A., Oraby, M.Y., Maimun, A., 2021. COLREGs compliant fuzzy-based collision avoidance system for multiple ship encounters. J. Mar. Sci. Eng. 9 (8), 790.

Arrichiello, F., Chiaverini, S., Fossen, T., 2006. Formation control of underactuated surface vessels using the null-space-based behavioral control. In: Proceedings of 2006 IEEE/RSJ International Conference on Intelligent Robots and Systems. Beijing, China, pp. 5942–5947.

Binder, B., Johansen, T., Imsland, L., 2019. Improved predictions from measured disturbances in linear model predictive control. J. Process Control 75, 86–106.

Campbell, S., Naeem, W., Irwin, G., 2012. A review on improving the autonomy of unmanned surface vehicles through intelligent collision avoidance manoeuvres. Annu. Rev. Control 36 (2), 267–283.

Chen, L., Hopman, H., Negenborn, R.R., 2018. Distributed model predictive control for vessel train formations of cooperative multi-vessel systems. Transp. Res. C 92, 101–118.

Chiang, H.-T.L., Tapia, L., 2018. COLREG-RRT: An RRT-based COLREGS-compliant motion planner for surface vehicle navigation. IEEE Robot. Automat. Lett. 3 (3), 2024–2031.

Cockcroft, A.N., Lameijer, J.N.F., 2003. Guide to the Collision Avoidance Rules. Elsevier.

Du, Z., Negenborn, R.R., Reppa, V., 2021a. Cooperative multi-agent control for autonomous ship towing under environmental disturbances. IEEE/CAA J. Automat. Sin. 8 (8), 1365–1379.

Du, Z., Reppa, V., Negenborn, R.R., 2020. Cooperative control of autonomous tugs for ship towing. In: Proceedings of the 21st IFAC World Congress. Berlin, Germany, pp. 14671–14676.

Du, Z., Reppa, V., Negenborn, R.R., 2021b. MPC-based COLREGS compliant collision avoidance for a multi-vessel ship-towing system. In: Proceedings of the European Control Conference. ECC'21, Rotterdam, the Netherlands.

Eoh, G., Do Jeon, J., Lee, B.H., 2016. Cooperative object transportation using virtual electric dipole field. Int. J. Mech. Eng. Robot. Res. 5 (1), 6–10.

Fink, J., Hsieh, M.A., Kumar, V., 2008. Multi-robot manipulation via caging in environments with obstacles. In: Proceedings of 2008 IEEE International Conference on Robotics and Automation. Pasadena, CA, USA, pp. 1471–1476.

Fossen, T.I., 2011. Handbook of Marine Craft Hydrodynamics and Motion Control. John Wiley & Sons, Chichester, West Sussex, UK.

Gimenez, J., Gandolfo, D.C., Salinas, L.R., Rosales, C., Carelli, R., 2018. Multi-objective control for cooperative payload transport with rotorcraft UAVs. ISA Trans. 80, 491–502.

Hagen, I.B., Kufoalor, D.K.M., Brekke, E.F., Johansen, T.A., 2018. MPC-based collision avoidance strategy for existing marine vessel guidance systems. In: 2018 IEEE International Conference on Robotics and Automation. ICRA, Brisbane, QLD, Australia.

Haseltalab, A., Negenborn, R.R., 2019. Model predictive maneuvering control and energy management for all-electric autonomous ships. Appl. Energy 251, 113308.

Hensen, H., 2003. Tug Use in Port: A Practical Guide. Nautical Institute, London, UK.

Hepworth, M., 2021. Collision Avoidance for Autonomous Inland Vessels using Stereovision (Master's Thesis). Delft University of Technology.

Hinostroza, M., Xu, H., Soares, C.G., 2019. Cooperative operation of autonomous surface vehicles for maintaining formation in complex marine environment. Ocean Eng. 183, 132–154.

Huang, Y., Chen, L., Chen, P., Negenborn, R.R., van Gelder, P., 2020. Ship collision avoidance methods: State-of-the-art. Saf. Sci. 121, 451–473.

Huang, Y., Chen, L., van Gelder, P., 2019. Generalized velocity obstacle algorithm for preventing ship collisions at sea. Ocean Eng. 173, 142–156.

Johansen, T.A., Perez, T., Cristofaro, A., 2016. Ship collision avoidance and COLREGS compliance using simulation-based control behavior selection with predictive hazard assessment. IEEE Trans. Intell. Transp. Syst. 17 (12), 3407–3422.

Kim, H., Kim, D., Kim, H., Shin, J.-U., Myung, H., 2016. An extended any-angle path planning algorithm for maintaining formation of multi-agent jellyfish elimination robot system. Int. J. Control Autom. Syst. 14 (2), 598–607.

Lee, T., 2015. Collision avoidance for quadrotor UAVs transporting a payload via Voronoi tessellation. In: Proceedings of 2015 American Control Conference. ACC, Chicago, IL, USA, pp. 1842–1848.

Lee, H., Kim, H., Kim, H.J., 2018. Planning and control for collision-free cooperative aerial transportation. IEEE Trans. Automat. Sci. Eng. 15 (1), 189–201.

Li, B., Zhang, Y., Acarma, T., Kong, Q., Zhang, Y., 2019. Trajectory planning for a tractor with multiple trailers in extremely narrow environments: A unified approach. In: Proceedings of 2019 International Conference on Robotics and Automation. ICRA, Montreal, QC, Canada, Canada, pp. 8557–8562.

Lyu, H., Yin, Y., 2018. COLREGS-constrained real-time path planning for autonomous ships using modified artificial potential fields. J. Navig. 72 (3), 588–608.

Negenborn, R.R., Maestre, J.M., 2013. On 35 approaches for distributed MPC made easy. In: Intelligent Systems, Control and Automation: Science and Engineering. Springer Netherlands, pp. 1–37.

Qin, Z., Lin, Z., Yang, D., Li, P., 2017. A task-based hierarchical control strategy for autonomous motion of an unmanned surface vehicle swarm. Appl. Ocean Res. 65, 251–261.

Raghuwaiya, K., Singh, S., Sharma, B.N., Vanualailai, J., 2014. Potential field functions for motion planning and posture of the standard 3-trailer system. Int. J. Math., Comput. Sci. Eng. 8 (3), 19–25.

Ren, W., Beard, R., Atkins, E., 2005. A survey of consensus problems in multi-agent coordination. In: Proceedings of the 2005, American Control Conference, 2005. Portland, OR, USA, pp. 1859–1864.

Rosales, C., Gimenez, J., Rossomando, F., Soria, C., Sarcinelli-Filho, M., Carelli, R., 2019. UAVS formation control with dynamic compensation using neuro adaptive SMC. In: Proceedings of 2019 International Conference on Unmanned Aircraft Systems. ICUAS, Atlanta, GA, USA, pp. 93–99.

Rossomando, F., Rosales, C., Gimenez, J., Salinas, L., Soria, C., Sarcinelli-Filho, M., Carelli, R., 2020. Aerial load transportation with multiple quadrotors based on a kinematic controller and a neural SMC dynamic compensation. J. Intell. Robot. Syst..

Skjetne, R., Smogeli, Ø., Fossen, T.I., 2004. Modeling, identification, and adaptive maneuvering of cybership II: A complete design with experiments. IFAC Proc. Vol. 37 (10), 203–208.

Stephen, B., Neal, P., Eric, C., Borja, P., Jonathan, E., 2010. Distributed optimization and statistical learning via the alternating direction method of multipliers. Found. Trends Mach. Learn. 3 (1), 1–122.

Tartaglione, G., D'Amato, E., Ariola, M., Rossi, P.S., Johansen, T.A., 2017. Model predictive control for a multi-body slung-load system. Robot. Auton. Syst. 92, 1–11.

Trym, T., Brekke, E.F., Johansen, T.A., 2020. On collision risk assessment for autonomous ships using scenario-based MPC. IFAC-PapersOnLine 53 (2), 14509–14516.

Veksler, A., Johansen, T.A., Borrelli, F., Realfsen, B., 2016. Dynamic positioning with model predictive control. IEEE Trans. Control Syst. Technol. 24 (4), 1340–1353.

Yuan, J., 2017. Hierarchical motion planning for multisteering tractor–trailer mobile robots with on-axle hitching. IEEE/ASME Trans. Mechatronics 22 (4), 1652–1662.

Zaccone, R., 2021. COLREG-compliant optimal path planning for real-time guidance and control of autonomous ships. J. Mar. Sci. Eng. 9 (4), 405.

Zhang, Q., Pan, W., Reppa, V., 2021. Model-reference reinforcement learning for collision-free tracking control of autonomous surface vehicles. IEEE Trans. Intell. Transp. Syst. 1–12.

Zips, P., Bock, M., Kugi, A., 2015. An optimisation-based path planner for truck-trailer systems with driving direction changes. In: Proceedings of 2015 IEEE International Conference on Robotics and Automation. ICRA, Seattle, WA, USA, pp. 630–636.